

A Quasi-periodic propagating wave and EUV waves excited simultaneously in a solar eruption event

Y. H. MIAO,^{1,2,3,4,5} Y. LIU,^{1,2,3,4} Y. D. SHEN,^{1,2} H. B. LI,^{1,5} Z. Z. ABIDIN,³ A. ELMHAMDI,⁴ AND A. S. KORDI⁴

¹*Yunnan Observatories, Chinese Academy of Sciences, Kunming, 650216, China*

²*Key Laboratory of Geospace Environment, Chinese Academy of Sciences, University of Science & Technology of China, Hefei 230026, China*

³*Radio Cosmology Lab, Department of Physics, Faculty of Science, University of Malaya, 50603 Kuala Lumpur, Malaysia.*

⁴*Department of Physics and Astronomy, King Saud University, PO Box 2455, Riyadh 11451, Saudi Arabia*

⁵*University of Chinese Academy of Sciences, Beijing 100049, China*

ABSTRACT

Quasi-periodic fast-propagating (QFP) magnetosonic waves and extreme ultraviolet (EUV) waves were proposed to be driven by solar flares and coronal mass ejections (CMEs), respectively. In this Letter, we present a detailed analysis of an interesting event in which we find that both QFP magnetosonic waves and EUV waves are excited simultaneously in one solar eruption event. The co-existence of the two wave phenomena offers an excellent opportunity to explore their driving mechanisms. The QFP waves propagate in a funnel-like loop system with a speed of 682–837 km s⁻¹ and a lifetime of 2 minutes. On the contrary, the EUV waves, which present a faster component and a slower component, propagate in a wide angular extent, experiencing reflection and refraction across a magnetic quasi-separatrix layer. The faster component of the EUV waves travels with a speed of 412–1287 km s⁻¹, whereas the slower component travels with a speed of 246–390 km s⁻¹. The lifetime of the EUV waves is ~15 minutes. It is revealed that the faster component of the EUV waves is cospatial with the first wavefront of the QFP wave train. Besides, The QFP waves have a period of about 45±5 seconds, which is absent in the associated flares. All these results imply that QFP waves can also be excited by mass ejections, including CMEs or jets.

Keywords: Sun: flares — Sun: corona — Sun: magnetic fields — Sun: oscillations - waves

1. INTRODUCTION

Waves are ubiquitous in the solar atmosphere, and have been investigated extensively. In the past several decades, various types of waves have been observed in the solar atmosphere, such as Moreton waves (Moreton 1960; Shen & Liu 2012a; Krause et al. 2018), coronal extreme-ultraviolet (EUV) waves (e.g., Thompson et al. 1998, 1999; Liu et al. 2010; Yang et al. 2013; Liu & Ofman 2014; Muhr et al. 2014; Shen et al. 2018c), slow (e.g., Nakariakov & Zimovets 2011) and fast (Ofman & Thompson 2002; Liu et al. 2011, 2012; Yuan et al. 2013; Zhang et al. 2015; Ofman & Liu 2018; Miao et al. 2018) modes magnetosonic waves. Besides these traveling waves, there exist various kinds of stationary waves trapped in coronal loops and filaments, which lead to coronal loop and filament oscillations (Nakariakov & Ofman 2001; Nakariakov & Verwichte 2005; Chen et al. 2008; Liu et al. 2012; Li & Zhang 2012; Shen et al. 2014a,b; Zhou et al. 2018). Waves and oscillatory phenomena in the solar atmosphere have been attractive since they are considered to be very important for coronal heating or be used to diagnose the magnetic field in which the waves are propagating (Nakariakov et al. 1999a,b; Nakariakov & Ofman 2001; Van Doorselaere et al. 2008; Chen 2009a; Shen et al. 2012, 2013; Ofman & Liu 2018; Shen et al. 2018c).

Large-scale extreme ultraviolet (EUV) waves were first detected by the Extreme-ultraviolet Imaging Telescope (EIT; Delaboudinière et al. 1995) aboard the *Solar Heliospheric Observatory*, and was originally called “EIT waves” (Thompson et al. 1998, 1999). In the past two decades, a large number of studies have been conducted to explore the physical nature and driving mechanism of this wave phenomenon. Regarding its physical nature, early researchers considered

that ‘‘EIT waves’’ are probably the coronal counterparts of the chromospheric Moreton waves, i.e., they are fast-mode waves or shock waves (Thompson et al. 1998, 1999; Wang 2000; Wu et al. 2001; Ofman & Thompson 2002; Schmidt & Ofman 2010; Shen & Liu 2012b; Shen et al. 2017b, 2018a,c). On the other hand, several non-wave models were suggested (Delannée 2000; Delannée et al. 2008; Liu et al. 2010, 2012). In particular, Chen et al. (2002, 2005) proposed that there should be two components of EUV waves associated with a coronal mass ejection (CME) event, i.e., a fast-mode wave (or shock wave) and a slowly moving apparent wave. Regarding the driving mechanism, some authors proposed that EUV waves are excited by the pressure pulse inside the flare (e.g., Khan & Aurass 2002; Hudson et al. 2003; Warmuth et al. 2004), while others considered that they are driven by CMEs or jets (e.g., Cliver et al. 1999; Chen et al. 2002; Chen 2009b; Li et al. 2012; Shen & Liu 2012b; Shen et al. 2017a). It is now generally believed that the large-scale EUV waves, either the faster component or the slower one, are driven by mass ejections, either CMEs or jets (see Warmuth 2015; Chen 2016, for reviews).

In recent years, another type of wave phenomenon, i.e., quasi-periodic fast-propagating (QFP) magnetosonic waves, became a hot topic, which was first reported by Liu et al. (2012) using high spatial and temporal resolution observations taken by the Atmospheric Imaging Assembly (AIA; Lemen et al. 2012) on board the *Solar Dynamics Observatory* (SDO; Pesnell et al. 2012). The QFP waves are observed as a wave train with multiple arc-shaped fronts, which propagate along funnel-like coronal loops. According to Liu & Ofman (2014), the period, speed, and deceleration of QFP waves are in ranges of 25–400 seconds, 500–2200 km s⁻¹, and 1–4 m s⁻², respectively. In the past seven years, many authors claimed that QFP waves have an intimate relationship with the accompanying flare and their initial positions are often seen to be in a few megameters from the flare kernel (Liu et al. 2011, 2012; Shen & Liu 2012a; Yuan et al. 2013; Kumar et al. 2017; Shen et al. 2018a,b). Ofman & Liu (2018) presented numerical simulations in order to understand the physics of QFP waves. Their simulation results tend to support that the pressure pulse inside a flare can generate QFP waves.

In this letter, we analyze a QFP wave and EUV waves that appeared simultaneously in the flare/CME event on 2011 March 10, which was captured by the SDO/AIA and the SDO Helioseismic and Magnetic Imager (HMI; Schou et al. 2012). Among the 10 wavelengths of the SDO/AIA, only the 171 Å (Fe IX; lg *T*=5.8) channel clearly showed the QFP wave, whereas the EUV waves can be seen in various EUV channels, in particular the 193 Å channel (Fe XII; lg *T*=6.1). We concentrate on the 171 Å and 193 Å channels in this study. Analysis results are introduced in Section 2, and conclusions and discussions are presented in Section 3. The co-existence of the two wave phenomena offers an excellent opportunity to explore their driving mechanisms.

2. RESULTS

A GOES C4.0 flare, whose start, peak, and end times were at about 06:40:00, 06:41:12, and 06:53:12 UT respectively, occurred in NOAA active region AR11166 on 2011 March 10. The CME was observed by *STEREO* spacecraft in two viewpoints¹ since about 06:50 UT. The morphology of the CME is similar to that in Patsourakos & Vourlidis (2009) and will be investigated in a separate paper. Here, we focus on the driving mechanisms of the QFP wave and the EUV waves. Note that this EUV wave event was not listed in the EUV wave catalog compiled by Nitta et al. (2013).

At about 06:40:38 UT, the first arc-shaped wavefront of the QFP wave was seen to propagate along the funnel-like loop system at the southeastern periphery of AR11166. The wavefront was visible for 2 minutes. Panel (a) of Figure 1 shows the overview of the QFP and EUV wave propagation coverage on the AIA 171 Å full-disk image, where several slices are chosen for plotting time-distance diagrams. We use a semi-automatic method to get time-distance diagrams from 15° wide sectors along A1–A6 on the solar surface (Podladchikova & Berghmans 2005; Liu et al. 2010; Long et al. 2011; Li et al. 2012). The same method is applied to sectors B1–B5, which are 10° wide. The red dotted curve (Cut C) shows the path of the QFP wave train, whereas the black, blue, and white lines represent the initial EUV waves, their reflection, and refraction, respectively. Panel (b) of Figure 1 shows the funnel-like loop system (L1) and the active region (see the black box). One can see a cluster of funnel-like loops rooted in AR11166. The QFP wave train is observed to propagate along L1 in the 171 Å images. It should be noted that the QFP wave could be observed only in the 171 Å channel along the funnel-like loop system (see L1 in panel(b) of Figure 1). With the SDO/AIA and *STEREO*/Ahead EUVI data and using the scc_measure.pro code in the standard Solar Software (SSW), we also measure the height of the funnel-like loop system, which is about 40 Mm.

¹ https://cdaw.gsfc.nasa.gov/movie/make_javamovie.php?img1=stb_co1s&img2=sta_co1s&stime=20110310_0400&etime=20110310_0800

The QFP and EUV waves morphologies and evolutions are displayed in Figure 2. Panels (a1)-(a6) and (b1)-(b6) are running difference images (i.e., from each image we subtract the one 12 seconds earlier) at 171 Å and 193 Å, respectively. At about 06:40:38 UT, the QFP wave was launched in the southeast of the AR11166 and its initial appearance position was about 36 Mm to the flare kernel. The start time of the QFP wave (06:40:38 UT) was slightly lagging behind the beginning of the accompanying flare (06:40:00 UT). Panel (a1) of Figure 2 shows the profiles of the wavefronts of the QFP wave, which are indicated by the green lines. In panel (b1) of Figure 2, the EUV wavefront can be seen clearly at 06:41:22 UT. The EUV wave front can also be seen in Figure 2(a2), as indicated by the shorter green line. We present an animation (animation.mpeg) to display the detailed evolution of the QFP and EUV waves in the online journal. Combining panels (a2) and (b1) of Figure 2, we find that the EUV wavefront is in juxtaposition with the first wavefront of the QFP wave train, which might indicate that the EUV wave is probably the counterpart of the first wavefront of the QFP wave train.

In panel (a3) of Figure 2, the relevant coronal structures are presented. The upper white arrow indicates the L1 loop system. The two red arrows indicate a magnetic separatrix surface (Thompson & Myers 2009; Liu et al. 2012; Schmidt & Ofman 2010). When the EUV wavefront approaches the magnetic separatrix surface, the wavefront became weaker and weaker, and then disappeared in the structure. About two minutes later (at about 06:45:12 UT), a new and small wavefront (see the green line in panels (a3)-(a4) of Figure 2) appeared to the southeast of the separatrix structure. Since there is no other erupting source around the magnetic separatrix structure, we suppose that the new wavefront is probably a refracted wave produced during the wave passage. In the meantime, a reflected wave is also observed to the north of the separatrix structure, which is indicated by the blue lines in Figure 2. The refraction and the reflection imply that the QFP wave and this primary EUV wave both have wave nature. A minute later (at about 06:46 UT), the propagation direction of the refracted wave changed when it passed through a remote magnetic structure (see the blue circle indicated by “P” in panel (a3) of Figure 2) near the AR11171. The refracted wavefront propagated in the southeast direction, and then gradually changed its direction to the east when passing through the strong magnetic structure indicated by “P”. The changing propagation direction of the wave suggests the refraction effect when passing through inhomogeneous coronal structures (Shen et al. 2013). The refracted wavefront is indicated by the red lines and observed in the AIA 171 and 193 Å images in Figure 2.

We use a semi-automatic method to study the detailed kinematics of the EUV waves, as well as the reflected and refracted waves. The details of the method can be seen in Liu et al. (2010); Long et al. (2011); Shen et al. (2013). Six sectors (A1–A6) are used to measure the behaviors of outgoing waves and reflected wave, and another five sectors (B1–B5) are used to measure the propagation of the refracted wave (see panel (a) of Figure 1). The results are presented in Figures 3 and 4. Figure 3 displays the time-distance diagrams of the AIA 171 Å and 193 Å running difference intensity along sectors A1–A6, where the two black dotted lines border the magnetic separatrix structure. The multiple parallel wave fronts in Figures 3(a1) and 3(b2) were also reported by Shen et al. (2019) and can be discerned in the numerical simulations of Chen et al. (2002). The propagation speeds of the primary wave along various sectors are in the ranges of 470–923 km s⁻¹ at 171 Å (see the red dotted lines in panels (a1)-(a5)) and 428–666 km s⁻¹ at 193 Å (see the black dotted lines in panels(b1)-(b6)). The speed of the refracted wave is about 1287 km s⁻¹ along sector A3, as revealed in Figure 3(a3). The apparent acceleration of the refracted wave could be caused by the change of the angle between the local wave vector and the sector direction. The speeds of the reflected waves, however, are only 78–131 km s⁻¹ at in the Å channel and 140–280 km s⁻¹ in the 193 Å channel, as indicated by the blue dotted lines in Figure 3. The strong reflection is due to the large gradient of the wave speeds (Schmidt & Ofman 2010; Liu et al. 2012; Shen et al. 2012). We also measure the propagation speeds of the refracted wave along sectors B1–B5, and the time-distance diagrams are displayed in Figure 4. One significant difference between Figures 4 and 3 is that two types of EUV waves can be discerned along slices B1–B5 in the AIA 171 Å waveband. The propagation speeds of the fast-component EUV waves are in the ranges of 412–742 km s⁻¹, whereas the propagation speed of the slow-component EUV waves are in the range of 229–385 km s⁻¹. Interestingly, only the slow-component EUV waves can be discernable in the 193 Å channel, with a travelling speed of 246–390 km s⁻¹ in Figure 4(b1–b4). The wave signal along sector B5 is very weak at 193 Å.

The kinematics of the QFP wavefronts is shown in panel (a6) of Figure 4 using the time-distance diagrams along the path of cut C marked in panel (a) of Figure 1. The diagram is made from the AIA 171 Å running difference images. The wave train started at about 06:40:38 UT. Four wave fronts can be identified from panel (a6) of Figure 4. The propagation speeds of the four wave fronts are obtained by fitting the corresponding ridges with straight lines. The speeds of the four wavefronts are 837, 750, 807, and 682 km s⁻¹, respectively. The lifetime of the QFP wave train was about 2 minutes. It was launched later than the flare, which was the same as previous reported QFP wave trains

(e.g., Liu et al. 2011; Shen & Liu 2012b; Yuan et al. 2013; Kumar et al. 2017). One important reason for many studies to support that QFP waves are strongly associated with flares is that the QFP waves have the same period as the flare kernels (Liu et al. 2011, 2012; Shen & Liu 2012b; Shen et al. 2018a,c). In order to obtain the period of the QFP wave train, we apply the wavelet analysis technique to the detrended intensity profile along the red dashed line (at a distance of 150 Mm) in Figure 4(a6). As revealed by Figure 5(a), the period of the QFP wave train is about 45 ± 5 seconds.

In order to better interpret the QFP waves and the EUV wave evolutions, an HMI longitudinal magnetogram overlaid with the coronal magnetic field lines extrapolated via the potential field source surface (PFSS Schatten et al. 1969; Schrijver & De Rosa 2003) model is displayed in Figure 5(b), where the green (white) lines represent the open (closed) fields. We present a cartoon to show the EUV wave propagation with the effects of reflection and refraction in panel (c) of Figure 5.

3. DISCUSSIONS AND CONCLUSIONS

QFP waves and EUV waves are both interesting phenomena observed in the solar corona. Generally, people considered that QFP waves have an intimate relationship with the accompanying flare (Liu et al. 2011, 2012; Shen & Liu 2012a; Yuan et al. 2013; Kumar et al. 2017; Shen et al. 2018a,b). This viewpoint was supported by the observational facts that the QFP waves have the same period as the intensity variation of the flare kernel and the wave fronts often propagate behind the CME frontal loop. On the contrary, although EUV waves also emanate from flaring active regions (Liu et al. 2012; Shen & Liu 2012a; Kumar & Manoharan 2013; Nisticò et al. 2014; Shen et al. 2018a), they, no matter the fast component or the slow component, are more tightly associated with CMEs (Chen et al. 2002; Patsourakos & Vourlidas 2009; Chen & Wu 2011; Chen et al. 2005; Zheng et al. 2016) or other types of mass eruptions, such as jets and expanding coronal loops (Shen et al. 2018b,c). Taking advantage of the high spatiotemporal resolution observations from SDO/AIA, we performed an observational study of a QFP wave train and an EUV wave that were simultaneously excited in one flare/CME eruption event that occurred on 2011 March 10 in the active region AR11166. The co-existence of the two types of waves provides an excellent opportunity to investigate the trigger mechanism of the QFP waves and EUV waves.

The QFP waves were propagating along a funnel-like loop system, with a period of about 45 ± 5 seconds. The speeds of the QFP waves were in the range of $682\text{--}837\text{ km s}^{-1}$. According to the online animation, we can see that the QFP wave train was only observed in the 171 \AA band, and was hardly visible in the 193 \AA band. In contrast, the EUV waves can be identified in different wavebands of the SDO/AIA observations. Along the sectors A1–A6 starting from the eruption source region, it seems that only the fast component of EUV waves was visible, with a travelling speed of $470\text{--}923\text{ km s}^{-1}$ in the 171 \AA waveband. According to Chen (2016), such a speed range is typical for the fast component of EUV waves. Hence it corresponds to the piston-driven shock wave ahead of the associated CME. Combining the animation and panels (a1) and (b1) of Figure 2, we believe that this EUV wavefront was in juxtaposition with the first wavefront of the QFP wave train. This implies that the fast-component of the EUV waves and the QFP wave train in this event originate from the same process, i.e., they are driven by the associated CME, rather than the pressure pulse in the associated flare kernels. Moreover, the period of the QFP wave train was about 45 ± 5 s, and such a period is absent in the light curve of the flare kernel. Therefore, we propose that CME-driven shock wave, when interacting with funnel-like coronal loops, may also drive QFP wave trains. In this scenario, the period of the QFP wave train is not associated with the fluctuating brightness of the flare kernels.

Besides, the effects of refraction and reflection are observed when the fast-component of the EUV wave interacted with a magnetic separatrix. The speeds of primary, reflected, and refracted waves are $428\text{--}923\text{ km s}^{-1}$, $78\text{--}280\text{ km s}^{-1}$, and $246\text{--}742\text{ km s}^{-1}$, respectively. Across the magnetic separatrix, the propagation direction of the wavefront gradually changed from southeastward to eastward. Uchida (1968) and Afanasyev & Uralov (2011) indicated that if a wave is a true fast-mode magnetosonic wave, refraction would veer the wave from regions with higher wave speeds toward regions with lower wave speeds. All above results are suggestive of that the EUV waves along sectors A1–A6 are true fast magnetosonic waves. According to the prediction of Chen et al. (2002, 2005), two types of EUV waves would be associated with a CME event, which was later confirmed by SDO/AIA observations (e.g., Chen & Wu 2011; Asai et al. 2012; Cheng et al. 2012; Kumar & Manoharan 2013). However, it should be noted that the two components of EUV waves do not always appear simultaneously, and only one component is evident in some events. In this paper, it seems that only the fast-component EUV wave appeared along sectors A1–A6. However, as revealed by Figure 4(a1–a5), two components of EUV waves can be clearly identified in the 171 \AA images, with the fast-component travelling with

a speed of 412–742 km s⁻¹, and the slow-component travelling with a speed of 229–385 km s⁻¹. The speed of the slow-component wave is roughly three times smaller than that of the fast-component EUV wave, as predicted by the magnetic field-line stretching model predicted by [Chen et al. \(2002, 2005\)](#).

In summary, QFP wave train and EUV waves in a single event was analyzed in this paper. It was revealed that the EUV wavefront was in juxtaposition with the first wavefront of the QFP wave train. **Hence, our finding confirms that QPF waves can be excited by CMEs.** During the interaction, the initial broadband pulse can dispersively evolve into multiple QFP wavefronts. [Pascoe et al. \(2013\)](#) presented simulation work that showed this process, and [Nisticò et al. \(2014\)](#) further confirmed the scenario via observation. Here, the broadband pulse could be regarded as a piston-driven shock wave as observed in the present case, which further dispersively evolved into the QFP wave along the funnel-like coronal loops. This scenario is different from that proposed by [Liu et al. \(2011\)](#) in that the period of the QFP wave train has nothing to do with the flare kernel. More events are required in order to understand what determines the period of the QFP wave train in this scenario.

We thank the excellent data provided by the *SDO* and *STEREO* teams. We also thank the referee for his/her valuable suggestions and comments that improved the quality of the letter. This work is funded by the grants from the National Scientific Foundation of China (NSFC 11533009) and from the Key Laboratory of Geospace Environment, CAS, University of Science and Technology of China. This work is also supported by the grant associated with project of the Group for Innovation of Yunnan Province and the Strategic Priority Research Program of CAS with grant XDA-17040507. The authors Y. Liu and Z.Z. Abidin would like to thank the University of Malaya Faculty of Science grant (GPF040B-2018) for their support. The research by A. Elmhamdi was supported by King Saud University, Deanship of Scientific Research, College of Science Research Center. In addition, we are also grateful to the One Belt and One Road project of the West Light Foundation, CAS.

REFERENCES

- Afanasyev, A. N., & Uralov, A. M. 2011, *SoPh*, 273, 479
- Asai, A., Ishii, T. T., Isobe, H., et al. 2012, *ApJL*, 745, L18
- Chen, P. 2009a, *Science in China: Physics, Mechanics and Astronomy*, 52, 1785
- Chen, P. F. 2009b, *ApJL*, 698, L112
- . 2016, Washington DC American Geophysical Union Geophysical Monograph Series, 216, 381
- Chen, P. F., Fang, C., & Shibata, K. 2005, *ApJ*, 622, 1202
- Chen, P. F., Innes, D. E., & Solanki, S. K. 2008, *A&A*, 484, 487
- Chen, P. F., Wu, S. T., Shibata, K., & Fang, C. 2002, *ApJL*, 572, L99
- Chen, P. F., & Wu, Y. 2011, *ApJL*, 732, L20
- Cheng, X., Zhang, J., Olmedo, O., et al. 2012, *ApJL*, 745, L5
- Cliiver, E. W., Webb, D. F., & Howard, R. A. 1999, *SoPh*, 187, 89
- Delaboudinière, J.-P., Artzner, G. E., Brunaud, J., et al. 1995, *SoPh*, 162, 291
- Delannée, C. 2000, *ApJ*, 545, 512
- Delannée, C., Török, T., Aulanier, G., & Hochedez, J.-F. 2008, *SoPh*, 247, 123
- Hudson, H. S., Khan, J. I., Lemen, J. R., Nitta, N. V., & Uchida, Y. 2003, *SoPh*, 212, 121
- Khan, J. I., & Aurass, H. 2002, *A&A*, 383, 1018
- Krause, G., Cécere, M., Zurbriggen, E., et al. 2018, *MNRAS*, 474, 770
- Kumar, P., & Manoharan, P. K. 2013, *A&A*, 553, A109
- Kumar, P., Nakariakov, V. M., & Cho, K.-S. 2017, *ApJ*, 844, 149
- Lemen, J. R., Title, A. M., Akin, D. J., et al. 2012, *SoPh*, 275, 17
- Li, T., & Zhang, J. 2012, *ApJL*, 760, L10
- Li, T., Zhang, J., Yang, S., & Liu, W. 2012, *ApJ*, 746, 13
- Liu, W., Nitta, N. V., Schrijver, C. J., Title, A. M., & Tarbell, T. D. 2010, *ApJL*, 723, L53
- Liu, W., & Ofman, L. 2014, *SoPh*, 289, 3233
- Liu, W., Ofman, L., Nitta, N. V., et al. 2012, *ApJ*, 753, 52
- Liu, W., Title, A. M., Zhao, J., et al. 2011, *ApJL*, 736, L13
- Long, D. M., Gallagher, P. T., McAteer, R. T. J., & Bloomfield, D. S. 2011, *A&A*, 531, A42
- Miao, Y., Liu, Y., Li, H. B., et al. 2018, *ApJ*, 869, 39
- Moreton, G. E. 1960, *AJ*, 65, 494
- Muhr, N., Veronig, A. M., Kienreich, I. W., et al. 2014, *SoPh*, 289, 4563
- Nakariakov, V. M., & Ofman, L. 2001, *A&A*, 372, L53
- Nakariakov, V. M., Ofman, L., Deluca, E. E., Roberts, B., & Davila, J. M. 1999a, *Science*, 285, 862

- Nakariakov, V. M., Roberts, B., & Murawski, K. 1999b, in *Astronomical Society of the Pacific Conference Series*, Vol. 184, *Third Advances in Solar Physics Euroconference: Magnetic Fields and Oscillations*, ed. B. Schmieder, A. Hofmann, & J. Staude, 243–247
- Nakariakov, V. M., & Verwichte, E. 2005, *Living Reviews in Solar Physics*, 2, 3
- Nakariakov, V. M., & Zimovets, I. V. 2011, *ApJL*, 730, L27
- Nisticò, G., Pascoe, D. J., & Nakariakov, V. M. 2014, *A&A*, 569, A12
- Nitta, N. V., Schrijver, C. J., Title, A. M., & Liu, W. 2013, *ApJ*, 776, 58
- Ofman, L., & Liu, W. 2018, *ApJ*, 860, 54
- Ofman, L., & Thompson, B. J. 2002, *ApJ*, 574, 440
- Pascoe, D. J., Nakariakov, V. M., & Kupriyanova, E. G. 2013, *A&A*, 560, A97
- Patsourakos, S., & Vourlidas, A. 2009, *ApJL*, 700, L182
- Pesnell, W. D., Thompson, B. J., & Chamberlin, P. C. 2012, *SoPh*, 275, 3
- Podladchikova, O., & Berghmans, D. 2005, *SoPh*, 228, 265
- Schatten, K. H., Wilcox, J. M., & Ness, N. F. 1969, *SoPh*, 6, 442
- Schmidt, J. M., & Ofman, L. 2010, *ApJ*, 713, 1008
- Schou, J., Borrero, J. M., Norton, A. A., et al. 2012, *SoPh*, 275, 327
- Schrijver, C. J., & De Rosa, M. L. 2003, *SoPh*, 212, 165
- Shen, Y., Ichimoto, K., Ishii, T. T., et al. 2014a, *ApJ*, 786, 151
- Shen, Y., & Liu, Y. 2012a, *ApJ*, 753, 53
- . 2012b, *ApJL*, 752, L23
- Shen, Y., Liu, Y., Song, T., & Tian, Z. 2018a, *ApJ*, 853, 1
- Shen, Y., Liu, Y., Su, J., & Deng, Y. 2012, *ApJ*, 745, 164
- Shen, Y., Liu, Y., Su, J., et al. 2013, *ApJL*, 773, L33
- Shen, Y., Liu, Y., Tian, Z., & Qu, Z. 2017a, *ApJ*, 851, 101
- Shen, Y., Liu, Y. D., Chen, P. F., & Ichimoto, K. 2014b, *ApJ*, 795, 130
- Shen, Y., Liu, Y. D., Su, J., Qu, Z., & Tian, Z. 2017b, *ApJ*, 851, 67
- Shen, Y., Tang, Z., Li, H., & Liu, Y. 2018b, *MNRAS*, 480, L63
- Shen, Y. D., Chen, P. F., Tang, Z. H., et al. 2019, *ApJ*, under review
- Shen, Y., Tang, Z., Miao, Y., Su, J., & Liu, Y. 2018c, *ApJL*, 860, L8
- Thompson, B. J., & Myers, D. C. 2009, *ApJS*, 183, 225
- Thompson, B. J., Plunkett, S. P., Gurman, J. B., et al. 1998, *Geophys. Res. Lett.*, 25, 2465
- Thompson, B. J., Gurman, J. B., Neupert, W. M., et al. 1999, *ApJL*, 517, L151
- Uchida, Y. 1968, *SoPh*, 4, 30
- Van Doorselaere, T., Nakariakov, V. M., & Verwichte, E. 2008, *ApJL*, 676, L73
- Wang, Y.-M. 2000, *ApJL*, 543, L89
- Warmuth, A. 2015, *Living Reviews in Solar Physics*, 12, 3
- Warmuth, A., Vršnak, B., Magdalenić, J., Hanslmeier, A., & Otruba, W. 2004, *A&A*, 418, 1117
- Wu, S. T., Zheng, H., Wang, S., et al. 2001, *J. Geophys. Res.*, 106, 25089
- Yang, L., Zhang, J., Liu, W., Li, T., & Shen, Y. 2013, *ApJ*, 775, 39
- Yuan, D., Shen, Y., Liu, Y., et al. 2013, *A&A*, 554, A144
- Zhang, Y., Zhang, J., Wang, J., & Nakariakov, V. M. 2015, *A&A*, 581, A78
- Zheng, R., Chen, Y., Du, G., & Li, C. 2016, *ApJL*, 819, L18
- Zhou, Y.-H., Xia, C., Keppens, R., Fang, C., & Chen, P. F. 2018, *ApJ*, 856, 179

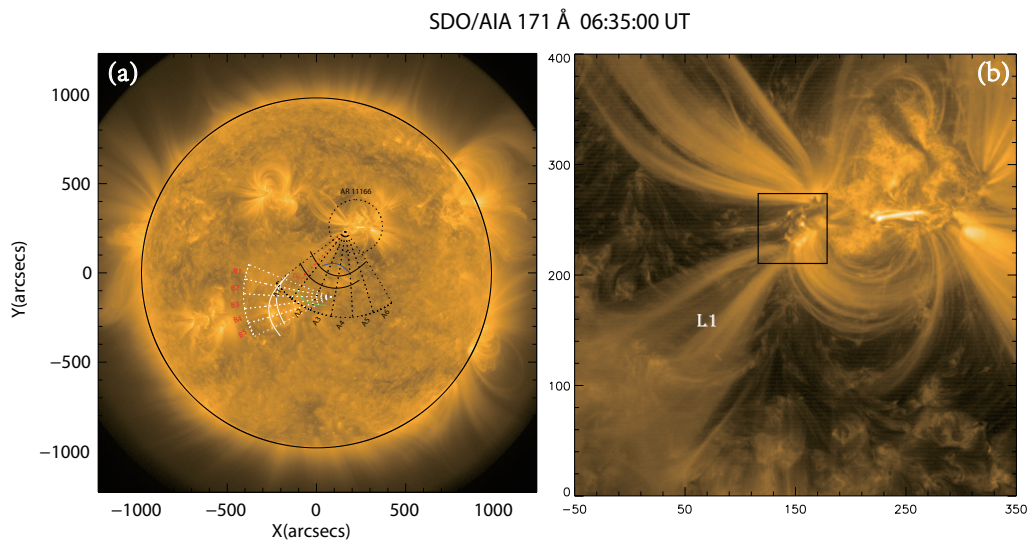


Figure 1. Panel (a): *SDO/AIA* 171 Å full-disk image shows six 15° (A1-A6), five 10° (B1-B5) wide sectors. The dotted curve (Cut C) presents the path used to obtain time-distance diagram. The black and blue lines represent the primary EUV wave and reflection, respectively. The green and white lines show the two refracted waves, respectively. Panel (b): the L1 represents the funnel-like loop system. The box displays the flare active region.

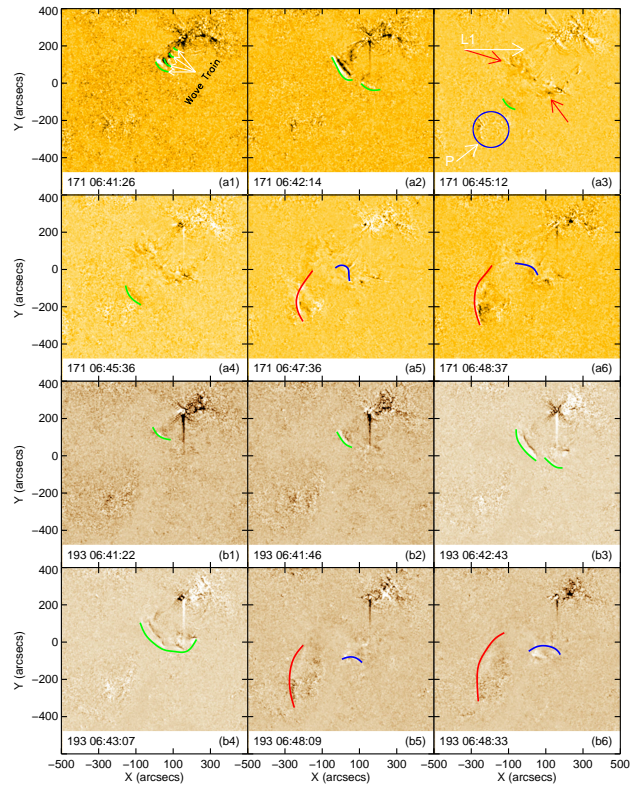


Figure 2. *SDO/AIA* 171 and 193 Å running difference images to show the QFP and the EUV wave evolutions. Four green lines represent the wavefronts of the QFP wave in panel (a1). The green lines display the EUV wave in panels (a2), (b1), (b2), (b3) and (b4). The green line represents the first refracted wave in panels (a3) and (a4). The blue circle indicates the magnetic structure (“P”) near the AR11171. The two arrows indicate the topological magnetic separatrix surface in panel (a3). The blue and red lines represent the reflected and the second refracted waves, respectively. An animation (animation.mpeg) can be seen in the online journal.

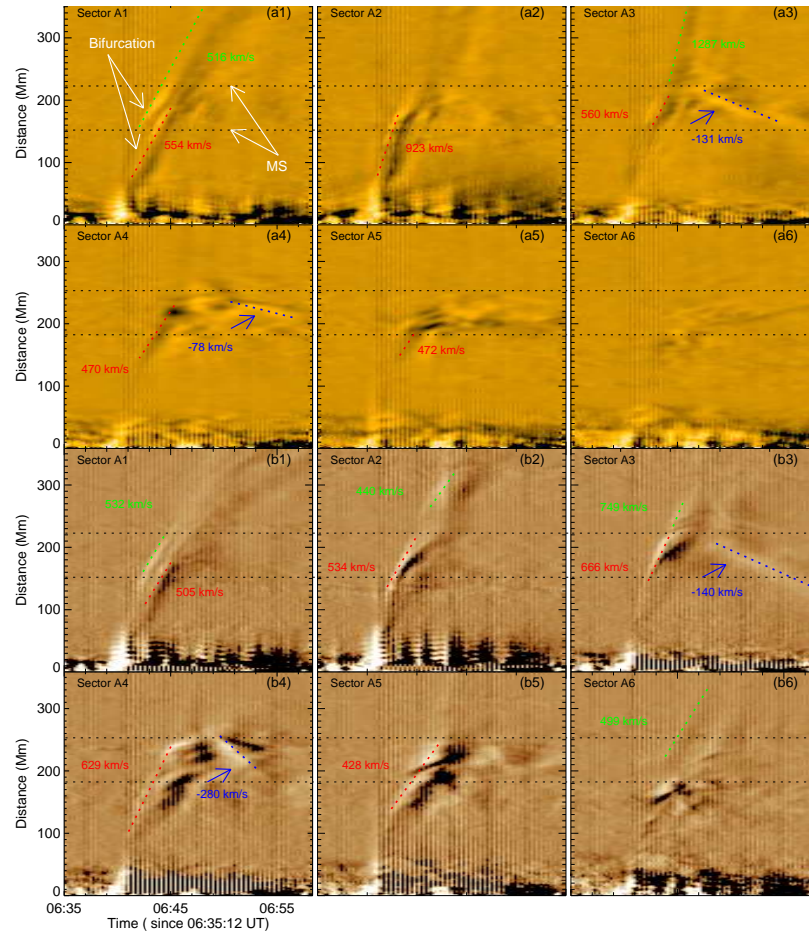


Figure 3. Panels (a1)-(a6) and (b1)-(b6) are time-distance diagrams obtained from AIA 171 and 193 Å running-difference images along sectors A1-A6, respectively. Between the two black dotted lines counterpart the topological magnetic separatrix (MS) surface structure. The speeds of the primary, refracted and reflected waves are present with different colors. The red dotted lines are the linear fit to the bright ridge produced before the interaction of the wave and the “MS”. The green dotted lines are the linear fit to the bright ridge produced after the interaction of the wave and the “MS”. The blue dotted lines are the linear fit to the bright ridge of the reflected wave.

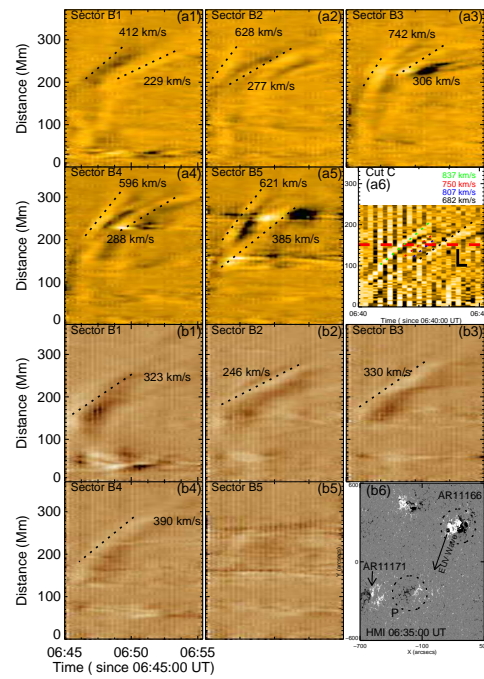


Figure 4. Panels (a1)-(a5) and (b1)-(b5) are time-distance diagrams obtained from AIA 171 and 193 Å running difference images along sectors B1-B5, respectively. Panel (a6) shows the time-distance diagram obtained from AIA 171 Å running-difference images along Cut C. The red-dashed line (L) in panel (a6) mark the position where we analyze the periodicity of the QFP wave. Panel (b6) simply shows magnetic configurations of AR11166 and the magnetic structure “P”. The red arrow indicates the direction of the initial wave propagates direction. The magnetic structure “P” represents the magnetic structure near the AR11171.

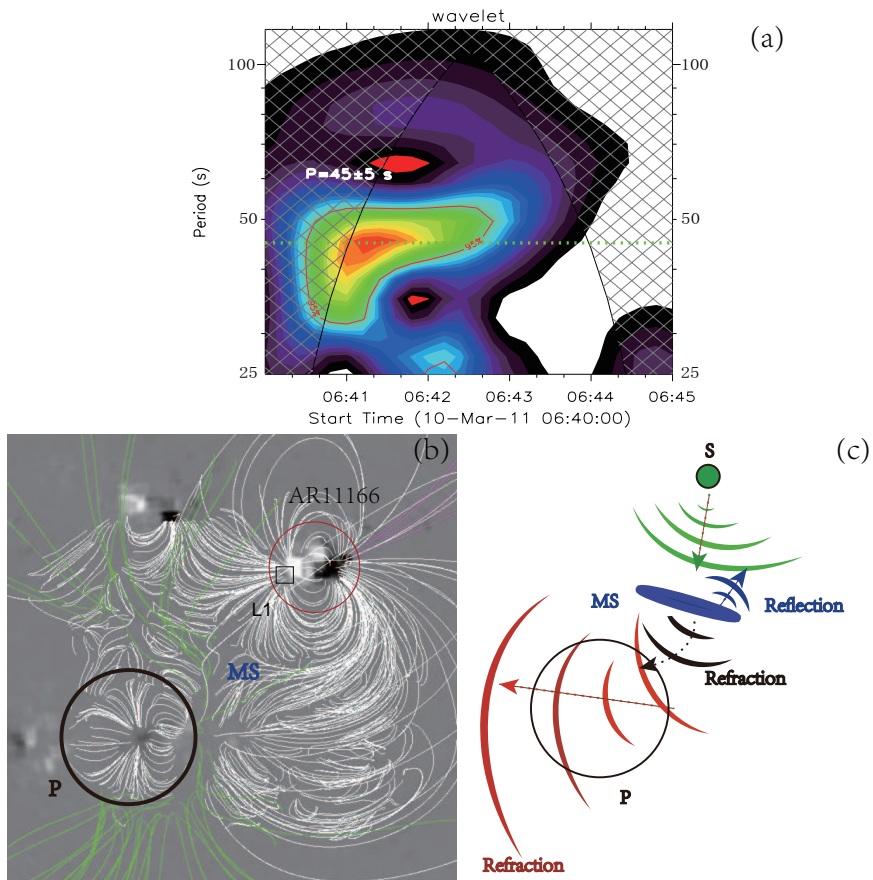


Figure 5. Panel (a) shows the period of the QFP wave. Panel (b) shows the coronal magnetic fields by using the PFSS model. The green lines represent open field and the white lines represent closed field. The black box shows the active region of initial flare eruption. Panel (c) presents a cartoon to further understand the evolutions of the EUV wave, the reflection and the refraction. The “S” represents the source of the wave. The magnetic structure “P” represents the remote magnetic structure that is enclosed by a black circle. The “MS” represents the topological magnetic separatrix surface.